Materials and Design 193 (2020) 108785

Contents lists available at ScienceDirect

Materials and Design

journal homepage: www.elsevier.com/locate/matdes

# 3D printing of multi-material composites with tunable shape memory behavior

Chao Yuan [a,1], Fangfang Wang [a,b,1], Biyun Qi [c], Zhen Ding [c,*], David W. Rosen [a,*], Qi Ge [d,*]

[a] Digital Manufacturing and Design Centre, Singapore University of Technology and Design, Singapore 487372, Singapore
[b] School of Civil Engineering, Xi'an University of Technology, Xi'an 710048, China
[c] CAS Key Laboratory of Health Informatics, Shenzhen Institutes of Advanced Technology, Chinese Academy of Sciences, Shenzhen 518055, China
[d] Department of Mechanical and Energy Engineering, Southern University of Science and Technology, Shenzhen 518055, China

## HIGHLIGHTS

- A layout design strategy is proposed to regulate the shape memory performance of multi-material composites.
- Theoretical analysis and finite element simulations are conducted to investigate the tunable shape memory performance.
- Composites of different material layouts are laminated into bilayer structures to achieve programmed active bending.

## GRAPHICAL ABSTRACT

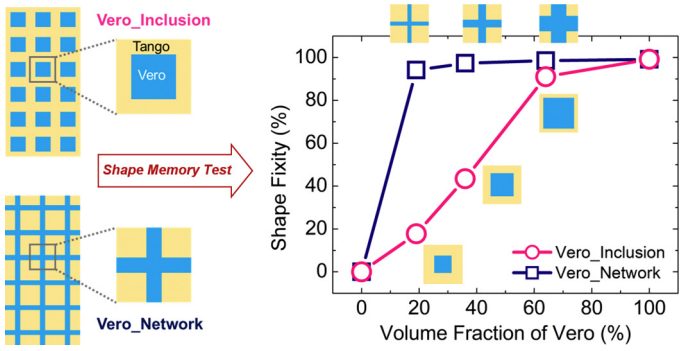


## ARTICLE INFO

*Article history:*
Received 25 March 2020
Received in revised form 3 May 2020
Accepted 4 May 2020
Available online 07 May 2020

*Keywords:*
3D printing
Shape memory polymer
Composite
Multi-material

## ABSTRACT

Three-dimensional (3D) printing has offered considerable convenience in fabricating functional structures constructed with shape memory polymers (SMPs). Conventionally, to meet the specific requirements for given applications, the shape memory property of a SMP is regulated by tailoring its molecular structure from the perspective of polymer chemistry. By virtue of the recent advances in multi-material 3D printing technology, new opportunities have emerged to customize the shape memory property from the perspective of composite material design. In this work, we propose a novel layout design strategy to 3D print multi-material composites incorporating heat-responsive SMP and flexible elastomer. Under a given volume ratio of SMP and elastomer, distinct shape memory performances are obtained for different material layouts. The underlying mechanisms are theoretically investigated based on the mechanics of composite materials and finite element (FE) simulations are conducted to provide quantitative predictions for the experimental results. As a demonstration, composites of different material layouts are used as building blocks to fabricate bilayer laminates where the incompatibility of shape fixity are pre-embedded to trigger the programmed active bending.

© 2018 Published by Elsevier Ltd. This is an open access article under the CC BY-NC-ND license (http://creativecommons.org/licenses/by-nc-nd/4.0/).

## 1. Introduction

Shape memory polymers (SMPs) are a typical group of active materials capable of achieving programmed shape memory effect in response to environmental stimuli [1–3]. By virtue of their high stiffness and rapid response speed, various SMP-based applications have been

* Corresponding authors.
*E-mail addresses:* zhen.ding@siat.ac.cn (Z. Ding), david_rosen@sutd.edu.sg (D.W. Rosen), geq@sustech.edu.cn (Q. Ge).
[1]These two authors contributed equally to this work.

https://doi.org/10.1016/j.matdes.2020.108785
0264-1275/© 2018 Published by Elsevier Ltd. This is an open access article under the CC BY-NC-ND license (http://creativecommons.org/licenses/by-nc-nd/4.0/).

demonstrated including actuators [4], flexible electronics [5,6], soft robotics [7–9], biomedical devices [10,11], and others. Among these applications, heat-responsive SMPs are the most commonly used category due to its convenience in practice. Generally, the material is first preprogrammed into a temporary fixed shape under thermomechanical loading and then automatically recovers to its permanent shape upon reheating.

Three-dimensional (3D) printing has offered considerable convenience in fabricating functional structures constructed with shape memory polymers. Conventionally, to meet the specific requirements for given applications, the shape memory property of SMP is regulated by tailoring its molecular structure from the perspective of polymer chemistry [12–18]. For example, Choong et al. [15] and Wu et al. [16] respectively developed different acrylate-based photopolymer systems which combine tert-Butyl acrylate (tBA) as monomer and different diacrylate as crosslinker for the laser scanning stereolithography (SLA) or digital light processing (DLP) 3D printing. By varying the crosslinker concentration, different thermomechanical and shape memory properties can be obtained. Chen et al. [18] designed polymer blends system which was applicable to fused deposition modeling (FDM) 3D printing and the shape memory property can be tuned by varying the mixing ratio of blend components. However, if multiple shape memory properties are required to be spatially distributed at different locations within one single 3D printed part, an additional material exchange system [19,20] or material mixing system [21,22] is necessary to facilitate the 3D printing. Recently, Kuang et al. [23] and Zhang et al. [24] proposed a grayscale DLP method to spatially regulate the curing degree of acrylate-based photopolymer resin. As a result, the shape memory property can be digitally controlled without apparatus modifications.

Towards the issue of regulating shape memory property, recent advances in multi-material 3D printing technology provide us new opportunities from the perspective of composite material design where multiple materials can be precisely placed in 3D space with predesigned material composition and layout to realize specific material property or functionality [25,26]. In this work, we propose a new layout design strategy to 3D print multi-material composites incorporating heat-responsive SMP and flexible elastomer. By varying the distribution and composition of the component materials within a composite, significantly different mechanical performances can be observed in the shape memory cycle, which demonstrates the feasibility of our strategy in customizing the shape memory property. With its effectiveness and convenience, our approach can be potentially applied in different research areas including 4D printing [27–33], metamaterials [34,35], biomimetic structures [36,37], and others.

The paper is organized as follows. In Section 2, the methods of multi-material 3D printing and material characterizations are detailed. In Section 3, shape memory performance and thermomechanical behavior of different layout designs are experimentally compared at varying material compositions. Moreover, qualitative theoretical analysis and quantitative finite element (FE) simulations are conducted to investigate the effect of material distribution and composition on the shape memory performance of the composite. Then, by employing the difference in shape fixity, composites of different material layouts are laminated into a bilayer structure to achieve programmed active bending. In Section 4, potential applications of different layout designs are proposed to suggest the outlook of our method. In Section 5, conclusions are given.

## 2. Materials and methods

The shape memory composites were directly printed by the commercial PolyJet multimaterial 3D printer (J750, Stratasys, Edina, MN, USA) which is capable of precisely placing multiple materials with a finest in-plane resolution of 200 μm. Before printing, the computer-aided design (CAD) file that specifies the layout of the shape memory composite is transmitted into the 3D printer through GrabCAD Print software. During printing, different polymeric ink droplets are simultaneously jetted from separated print heads which are preheated to ~65 °C. After being deposited onto the building tray, the ink droplets are wiped into a smooth film by the roller and photocured by ultraviolet (UV) light. Once a layer is formed, the building tray moves down by ~30 μm to print the next layer.

Two commercial photopolymers VeroBlack and TangoPlus were respectively used as SMP and elastomer to construct the composites. At room temperature, VeroBlack behaves like a rigid plastic which is polymerized by isobornyl acrylate, acrylic monomer, urethane acrylate, epoxy acrylate, acrylic monomer, acrylic oligomer, and photo initiator. For TangoPlus, it behaves like a flexible rubber which is polymerized by urethane acrylate oligomer, exo-1,7,7-trimethylbicyclo hept-2-yl acrylate, methacrylate oligomer, polyurethane resin, and photo initiator.

Shape memory characterizations and dynamic mechanical analysis (DMA) of the printed composites were both conducted on the dynamic mechanical analyzer (Model Q800, TA Instruments, New Castle, DE, USA) in a uniaxial tension mode. Accordingly, the testing samples were designed into rectangular strips with a dimension of 15 mm × 3 mm × 0.5 mm.

Before the shape memory test, simple uniaxial tension was performed at 80 °C for each sample in a stress control mode to determine the loading stress $\sigma_0$ at which the strain reaches 5%. Then we initiated the shape memory cycle by equilibrating the sample at 80 °C for 10 min followed by loading it at a constant rate of 0.1 MPa/min until the stress reached $\sigma_0$. Subsequently, the temperature was linearly decreased at a rate of 2 °C/min while the stress $\sigma_0$ was maintained. After reaching 20 °C, the external force was instantaneously released and a temporary shape was obtained. At last, free recovery was triggered by reheating the sample from 20 °C to 80 °C at a rate of 2 °C/min.

For the DMA test, a sample was first equilibrated at 100 °C for 10 min while a constant load of 1 mN was maintained to prevent the sample from buckling induced by temperature variation. Then a sinusoidal strain with an amplitude of 0.1% was applied on the sample at a frequency of 1 Hz, and the temperature was linearly decreased from 100 °C to −50 °C at a rate of 2 °C/min. The storage modulus and loss factor (tan$\delta$) were recorded as a function of temperature, and the glass transition temperature ($T_g$) was identified to be the temperature at which the maximum tan$\delta$ value was located.

## 3. Results

### 3.1. Shape memory behavior and dynamic mechanical analysis

The temperature-dependent strain response of VeroBlack within a full shape memory cycle is shown in Fig. 1a. To quantify the material's ability of fixing the programmed shape, we define the shape fixity

$$f = \varepsilon_{fix}/\varepsilon_{programme} \tag{1}$$

where $\varepsilon_{fix}$ and $\varepsilon_{programme}$ respectively denote the temporarily fixed strain at 20 °C and the programmed strain at 80 °C. As shown in Fig. 1a, since the strain programmed at 80 °C is almost fully retained by the temporary configuration after unloading at 20 °C, the shape fixity is nearly 100% for the tested VeroBlack. On the other hand, upon reaching the temporary configuration, shape memory effect is then demonstrated by reheating the VeroBlack sample to 80 °C where the original shape is fully recovered.

From the perspective of polymer physics, the shape memory behavior shown in Fig. 1a can be attributed to the glass transition phenomenon where polymers reversibly transform between glassy state and rubbery state. As shown in Fig. 1b, the storage modulus of VeroBlack increases by about two orders of the magnitude when the material is cooled from the rubbery state to the glassy one. At the rubbery state, instantaneous shape recovery can be realized upon unloading due to the entropic elasticity and high mobility of

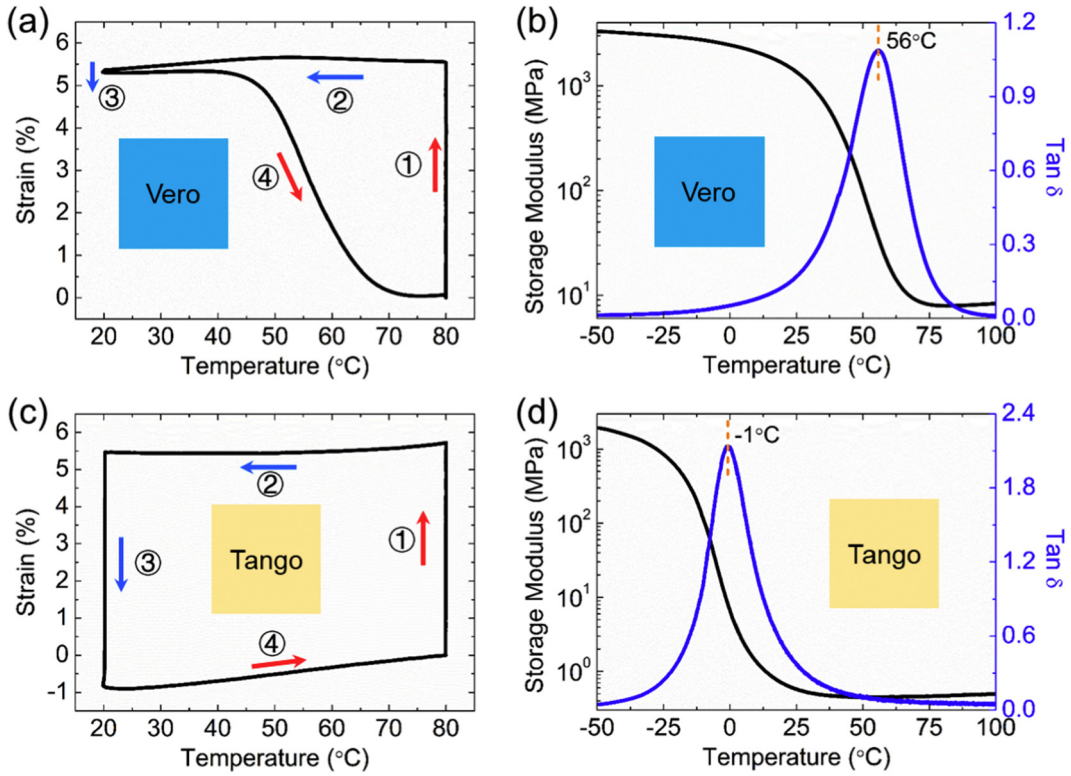


**Fig. 1.** Experimental characterizations of the shape memory behavior and thermomechanical properties for the base materials. a) Temperature-dependent strain response of VeroBlack in a full shape memory cycle. b) DMA results of VeroBlack. c) Temperature-dependent strain response of TangoPlus in a full shape memory cycle. d) DMA results of TangoPlus.

polymer chains. However, at the glassy state where the polymer chain mobility is significantly reduced, the unloaded material takes much longer time (years, even longer) to recover to its undeformed shape. The heating from 20 °C to 80 °C endows high mobility to the polymer chains, and enables the material to recover to its undeformed shape at the lab time scale.

In sharp contrast to VeroBlack, however, the strain incurred by TangoPlus at 80 °C is totally recovered upon unloading at 20 °C (Fig. 1c). This can be explained from the DMA result shown in Fig. 1d where the $T_g$ (−1 °C) of TangoPlus is far below the programming temperature range (20–80 °C) so that the material is still in its rubbery state even after cooling to 20 °C, and high polymer chain mobility and

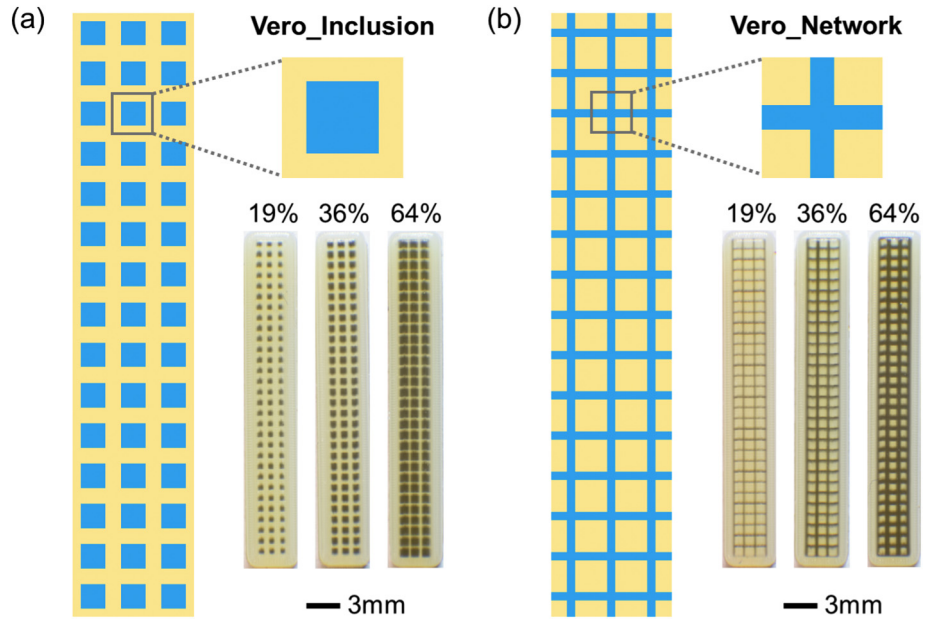


**Fig. 2.** Design schematics and sample photos of the shape memory composites. a) Vero_Inclusion design. b) Vero_Network design.

entropic elasticity lead to the instantaneous shape recovery after unloading.

With the understanding of the basic material properties, two types of composites were designed with same material composition but different material layouts. For the first type (Fig. 2a), VeroBlack is used as the embedded inclusion which is surrounded by TangoPlus. To investigate the effect of material composition on the shape memory performance of the composites, three VeroBlack volume fractions including 19%, 36% and 64% were selected as the representative compositions to build the experiment samples. For the second type (Fig. 2b), in contrast to the pattern shown in Fig. 2a, we exchange the roles of VeroBlack and TangoPlus in the composite where VeroBlack are connected into a network to separate the TangoPlus inclusions. Similarly, three representative VeroBlack compositions (19%, 36% and 64%) are designed. For clarity, we respectively refer to the material layouts shown in Fig. 2a and b as Vero_Inclusion design and Vero_Network design in the following sections.

Shape memory behavior of the multi-material composites are demonstrated in Fig. 3. With a low VeroBlack volume fraction (for instance, 19%), significant difference is observed in the temperature dependent strain curves between the layouts of Vero_Inclusion and Vero_Network. It is seen in Fig. 3a that upon unloading at 20 °C, over 80% of the strain is recovered for the Vero_Inclusion design, which indicates a poor shape fixity. However, if we convert the same amount of VeroBlack into a connected network, the recovered strain is reduced to below 10%. This sharp contrast reveals that the shape memory behavior of the multi-material composites is highly dependent on the layout of the component materials. Upon further increasing the VeroBlack volume fraction to 36%, the difference in the shape memory performance is reduced between the Vero_Inclusion and Vero_Network design. As shown in Fig. 3b, upon unloading, over 40% of the programming strain is able to be fixed by the Vero_Inclusion pattern. Compared to the earlier case where the VeroBlack volume fraction is 19%, the fixed strain has approximately doubled for the Vero_Inclusion pattern whereas superior shape fixity is consistently maintained by the Vero_Network pattern. When the VeroBlack volume fraction is increased into 64%, the pre-programmed strain fixed by the Vero_Inclusion pattern exceeds 80%, which further narrows the gap with Vero_Network pattern (Fig. 3c).

As a summary, the relationship between the shape fixity and VeroBlack volume fraction for both material layouts are shown in Fig. 3d. It is seen that for the Vero_Inclusion pattern, the shape fixity of the composite monotonically increases with the VeroBlack volume fraction. In contrast, the shape fixity of Vero_Network pattern is almost independent of the material composition by maintaining a high level. Furthermore, in addition to the DMA results shown in Fig. S3, the tunable shape memory property was also demonstrated with simple bending tests. The detailed experimental results could be found in Section S1 of the Supplementary Materials.

The sharp contrast of the shape memory performance between two layout designs can be qualitatively analyzed based on the mechanics of composite materials. As demonstrated in Fig. 1, VeroBlack shows a good shape fixity with almost all the programmed strain being fixed upon unloading, whereas TangoPlus behaves as an elastomer which is incapable of shape fixing. Therefore, for the composites incorporating VeroBlack and TangoPlus, the magnitude of the fixed deformation upon unloading is approximately equal to the deformation incurred by the VeroBlack components at 80 °C.

As shown in Fig. 4, representative volume elements (RVEs) of the Vero_Network and Vero_Inclusion patterns are schematically illustrated to facilitate the mechanical analysis. For the Vero_Network pattern (Fig. 4a), since the highlighted VeroBlack patch runs through the entire pattern along the loading direction, the fixed strain $\varepsilon_f^{Network}$

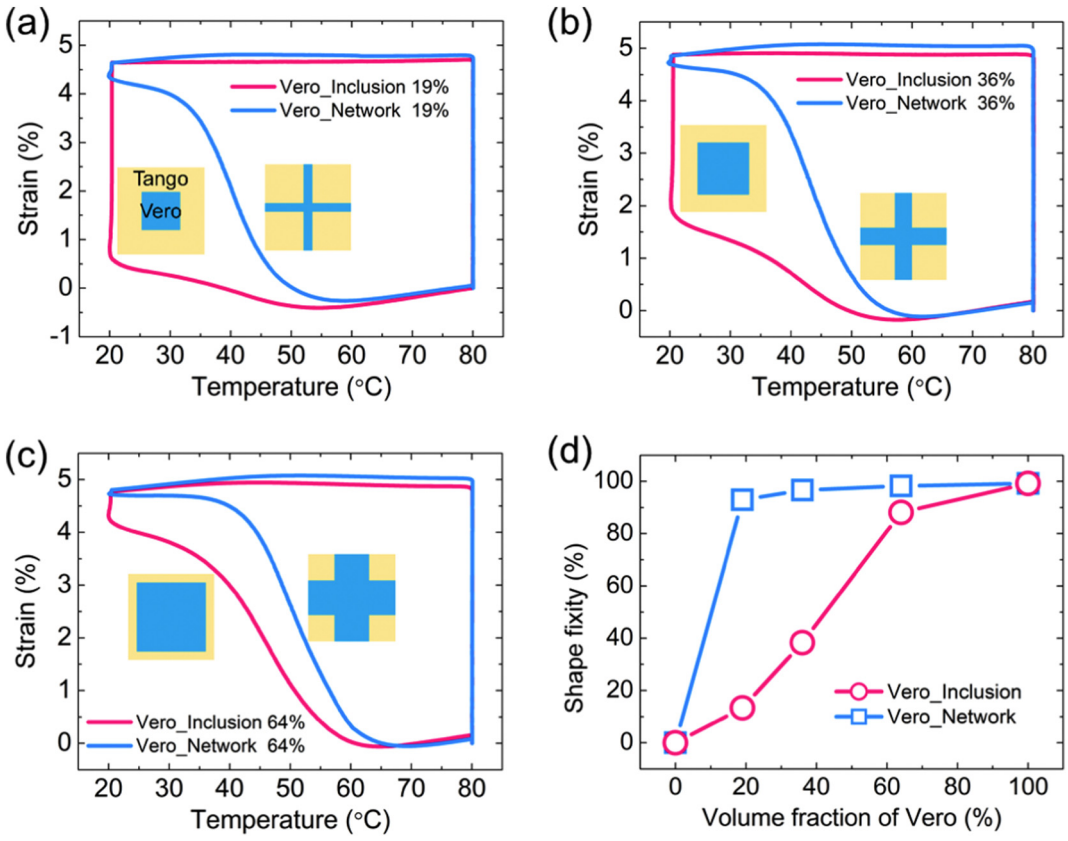


**Fig. 3.** Comparison of the shape memory performance for the multi-material composites with different material composition. a) 19% VeroBlack volume fraction. b) 36% VeroBlack volume fraction. c) 64% VeroBlack volume fraction. d) Comparison of the shape fixity at elevated VeroBlack volume fraction.

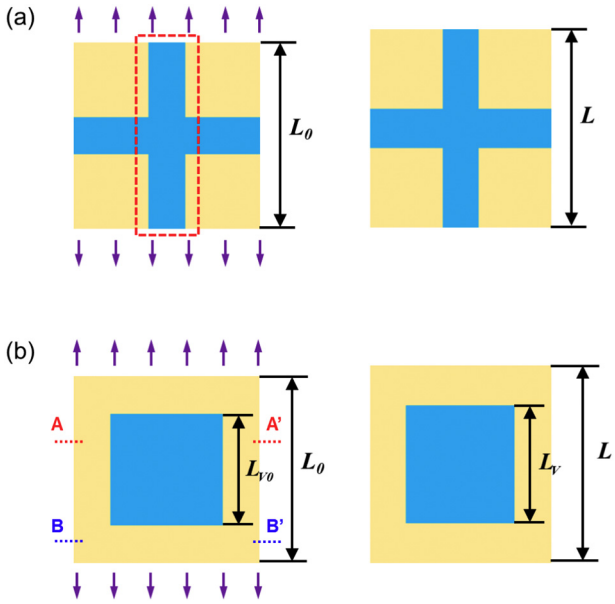


**Fig. 4.** Schematics of the representative volume elements (RVEs) of the multi-material composites. a) Vero_Network pattern. b) Vero_Inclusion pattern.

upon unloading is equal to the programming strain $\varepsilon_0$ incurred by the entire RVE and calculated by

$$\varepsilon_f^{Network} = \varepsilon_0 = (L - L_0)/L_0 \tag{2}$$

where $L_0$ and $L$ respectively represent the original and deformed length of the RVE along the loading direction. As indicated in Eq. (2), the strain fixed by the Vero_Network pattern is independent of the VeroBlack content and the corresponding shape fixity is always equal to 100%.

Compared to the Vero_Network pattern, the case of Vero_Inclusion pattern shown in Fig. 4b is a bit more complicated. Upon programming, the original RVE (dimension $L_0 \times L_0$) with a square VeroBlack inclusion (dimension $L_{V0} \times L_{V0}$) is deformed into a new configuration where the lengths of RVE and inclusion respectively increase to $L$ and $L_V$ along the loading direction. By considering the force balance between the cross sections of A-A' and B-B′ and adopting the small-strain assumption, we have

$$E_V \frac{L_V - L_{V0}}{L_{V0}} L_{V0} + E_T \frac{L_V - L_{V0}}{L_{V0}} (L_0 - L_{V0}) = E_T \frac{(L - L_V) - (L_0 - L_{V0})}{L_0 - L_{V0}} L_0 \tag{3}$$

where $E_V$ and $E_T$ represent the rubbery modulus of VeroBlack and TangoPlus. Since the volume fraction of VeroBlack can be calculated by $f = (L_{V0}/L_0)^2$, Eq. (3) can be rewritten into

$$\left[\frac{E_V}{E_T}\sqrt{f} + \frac{L_V - L_{V0}}{L_{V0}}\left(1 - \sqrt{f}\right)\right]\frac{L_V - L_{V0}}{L_{V0}} = \frac{(L - L_V) - (L_0 - L_{V0})}{L_0 - L_{V0}}. \tag{4}$$

By assuming VeroBlack inclusion is able to fix all the deformation incurred on itself, the fixed strain of the RVE upon unloading is calculated by

$$\varepsilon_f^{Inclusion} = (L_V - L_{V0})/L_0 \tag{5}$$

Upon solving $L_V$ from Eq. (4) and substituting it into Eq. (5), $\varepsilon_f^{Inclusion}$ is rewritten into

$$\varepsilon_f^{Inclusion} = \frac{\varepsilon_0}{\left(1 - \sqrt{f}\right)(E_V/E_T - 1) + 1/\sqrt{f}} \tag{6}$$

where the initial programming strain $\varepsilon_0$ incurred by the entire RVE is calculated by$\varepsilon_0 = (L - L_0)/L_0$. As indicated in Eq. (6), with the increase of inclusion content $f$, the fixed strain of the RVE is monotonically increased, which agrees with the trend of the experimental results shown in Fig. 3d. Herein, it is worth noting that the motivation of the above mechanical analysis is to provide qualitative explanations for the effects of material layout and composition on the shape fixity of the multi-material composites. For simplicity, the strain field is idealized into a one dimensional circumstance where the interaction between VeroBlack and TangoPlus is neglected.

On the other hand, we can view the multi-material composite as a new bulk material whose shape memory performance is dependent on the glass transition behavior. The DMA results of the multi-material composites with different material layouts and compositions are presented in Fig. 5. When the VeroBlack volume fraction is 19% (Fig. 5a), the tanδ curve of the Vero_Inclusion pattern shows a single peak at the vicinity of 2 °C. Similar to the case of pure TangoPlus shown in Fig. 1d, the temperature range (20–80 °C) of the shape memory programming is above the $T_g$ of the composites so that the glass transition is not triggered. As a result, upon decreasing the temperature from 80 °C to 20 °C, the composite consistently behaves in the rubbery state and the storage modulus barely increases, which directly leads to the poor shape fixity exhibited in the shape memory cycle shown in Fig. 3a.

For the Vero_Network pattern with the same VeroBlack content (Fig. 5b), two peaks are observed in the tanδ curve, one of which locates at the vicinity of 50 °C. Upon decreasing the temperature from 80 °C to 20 °C, the storage modulus increases by approximately two orders of the magnitude, which indicates the occurrence of glass transition. Therefore, good shape fixity can be observed in the shape memory cycle shown in Fig. 3a.

By further elevating the VeroBlack content, the Vero_Inclusion pattern and Vero_Network pattern exhibit different responses. As shown in Fig. 5c and e where the Vero_Inclusion pattern possesses higher VeroBlack content (36% and 64%), the tanδ peak continuously moves towards the high temperature and the storage modulus respectively increases by 6 and 52 times upon cooling from 80 °C to 20 °C. Since the degree of glass transition is gradually increased by enlarging the size of the embedded VeroBlack inclusion, the shape fixity of the Vero_Inclusion composite is accordingly enhanced (Fig. 3d). However, for the Vero_Network pattern shown in Fig. 5d and f, the location of the tanδ peak is hardly changed and the modulus increment maintains at the level of two orders of the magnitude. Therefore, regardless of the VeroBlack content, good shape memory performance is always observed, as shown in Fig. 3b and c.

The variation of the tanδ curve can be explained based on the energy dissipation status of different phases. Upon applying the oscillatory strain to the Vero_Inclusion sample with low Vero content (for instance, Vero_Inclusion 19% shown in Fig. 5a), the Vero inclusion is hardly deformed and almost all the deformation occurs in the connected Tango network. Therefore, energy dissipation is dominated by the Tango phase whose molecular chains manage to overcome the friction induced by intermolecular motion. However, As indicated by Eq. (6), with the increase of Vero content, more deformation is shared by the Vero inclusion phase which is accordingly more engaged in the energy dissipation. Since Vero possesses a much stiffer molecular network and higher crosslinking density than Tango, more energy input is required to release its frozen molecular chains and empower them with the mobility. Therefore, with the increase of Vero content, the tanδ peak which corresponds to the maximum energy dissipation shifts to higher temperature.

For the Vero_Network pattern where the Vero phase maintains the connected state, the Vero phase is always deformed and engaged in the energy dissipation regardless of the content. Therefore, two peaks can be always observed in the tanδ curve. The major one located at high temperature corresponds to the energy dissipation of Vero phase while the minor one located at low temperature corresponds to the

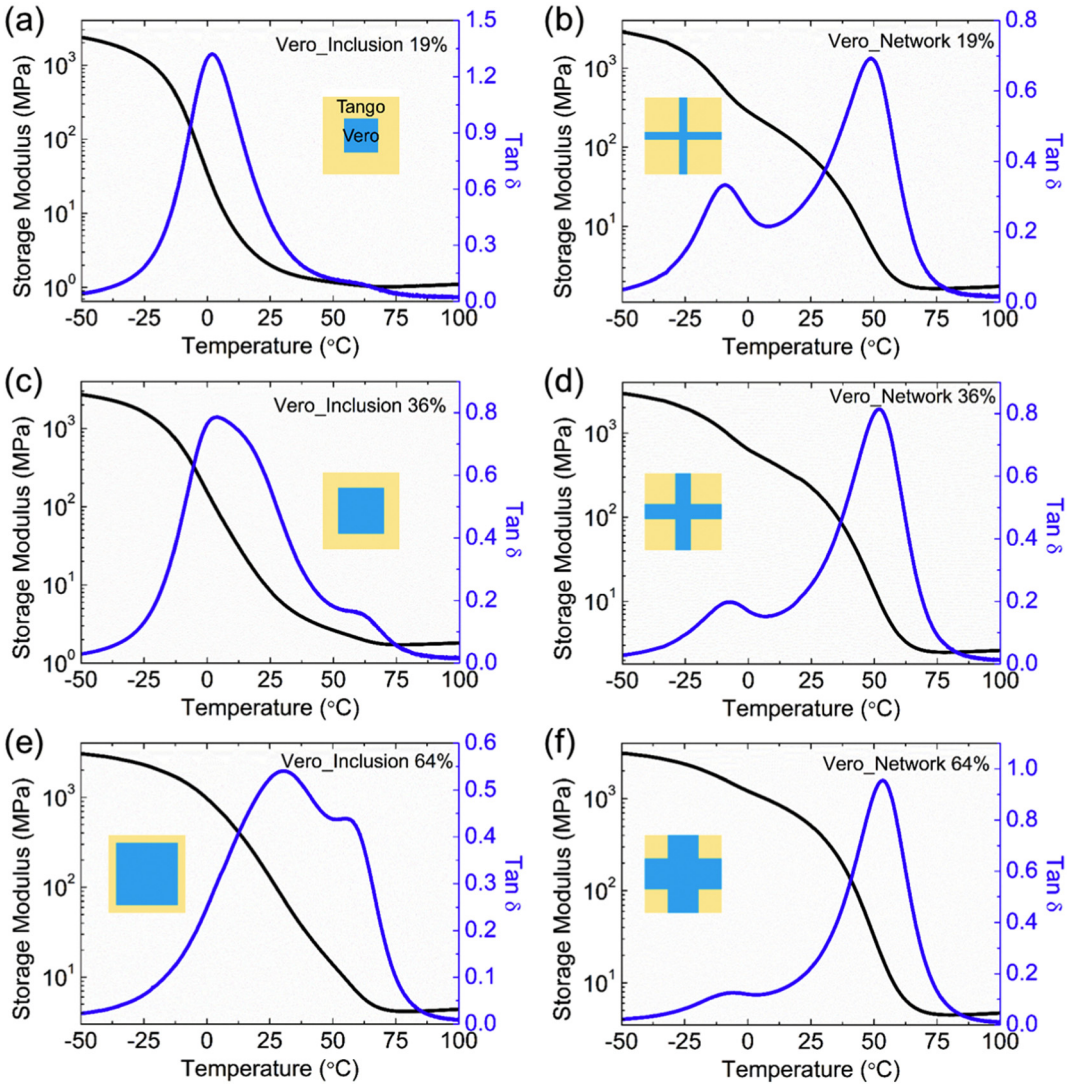


**Fig. 5.** DMA results of the multi-material composites with different material layouts and compositions. a) Vero_Inclusion pattern with a VeroBlack volume fraction of 19%. b) Vero_Network pattern with a VeroBlack volume fraction of 19%. c) Vero_Inclusion pattern with a VeroBlack volume fraction of 36%. d) Vero_Network pattern with a VeroBlack volume fraction of 36%. e) Vero_Inclusion pattern with a VeroBlack volume fraction of 64%. f) Vero_Network pattern with a VeroBlack volume fraction of 64%.

energy dissipation of Tango phase. Upon increasing the Vero content, since more molecular chains in the Vero phase are involved in the energy dissipation, a higher temperature is required to provide more energy to activate the increasing amount of frozen chains. Accordingly, a slight shift to higher temperature is observed in the tanδ peak.

### 3.2. Finite element simulations

In addition to the qualitative theoretical analysis given in Section 3.1, finite element (FE) simulations are performed in this section to quantitatively predict the shape memory behavior of the composites with different material layouts.

By using the commercially available FE software package ABAQUS (Dassault Systems, Johnston, RI, USA), two-dimensional (2D) square representative volume elements (RVEs) with Vero_Network and Vero_Inclusion patterns are respectively built and constrained by periodic boundary conditions. Since the Vero components may experience glass transition during the shape memory cycle, a multi-branch spring-dashpot constitutive model [38] is used to describe its time and temperature dependent thermoviscoelastic behavior. In this model, a number of Maxwell elements consisting of spring and dashpot are arranged in parallel and the viscosity of the dashpot is assumed to follow the time-temperature superposition principle (TTSP). FE implementation of the constitutive model is achieved by providing the ABAQUS built-in Prony-series model with the fitted spring and dashpot parameters (given in Table S1 of the Supplementary Materials) in the time domain and programming a UTRS subroutine to define the TTSP relationship. More details regarding the constitutive model and parameter characterizations can be found in Section S2 of the Supplementary Materials. On the other hand, since Tango consistently behaves in the rubbery state during the shape memory cycle, a linear elastic model is sufficient to describe its mechanical behavior. The loading and temperature boundary conditions are maintained consistent with the actual experiments and coupled temperature-displacement analysis is conducted. CPE4HT elements in the ABAQUS element library are used to mesh the entire RVE.

FE simulation results of the strain variation in a full shape memory cycle are compared with their respective experimental measurements for both Vero_Inclusion pattern (Fig. 6a–c) and Vero_Network pattern (Fig. 6d–f). It is seen that for all tested cases, the FE simulations can capture the experimental curves with reasonable accuracy.

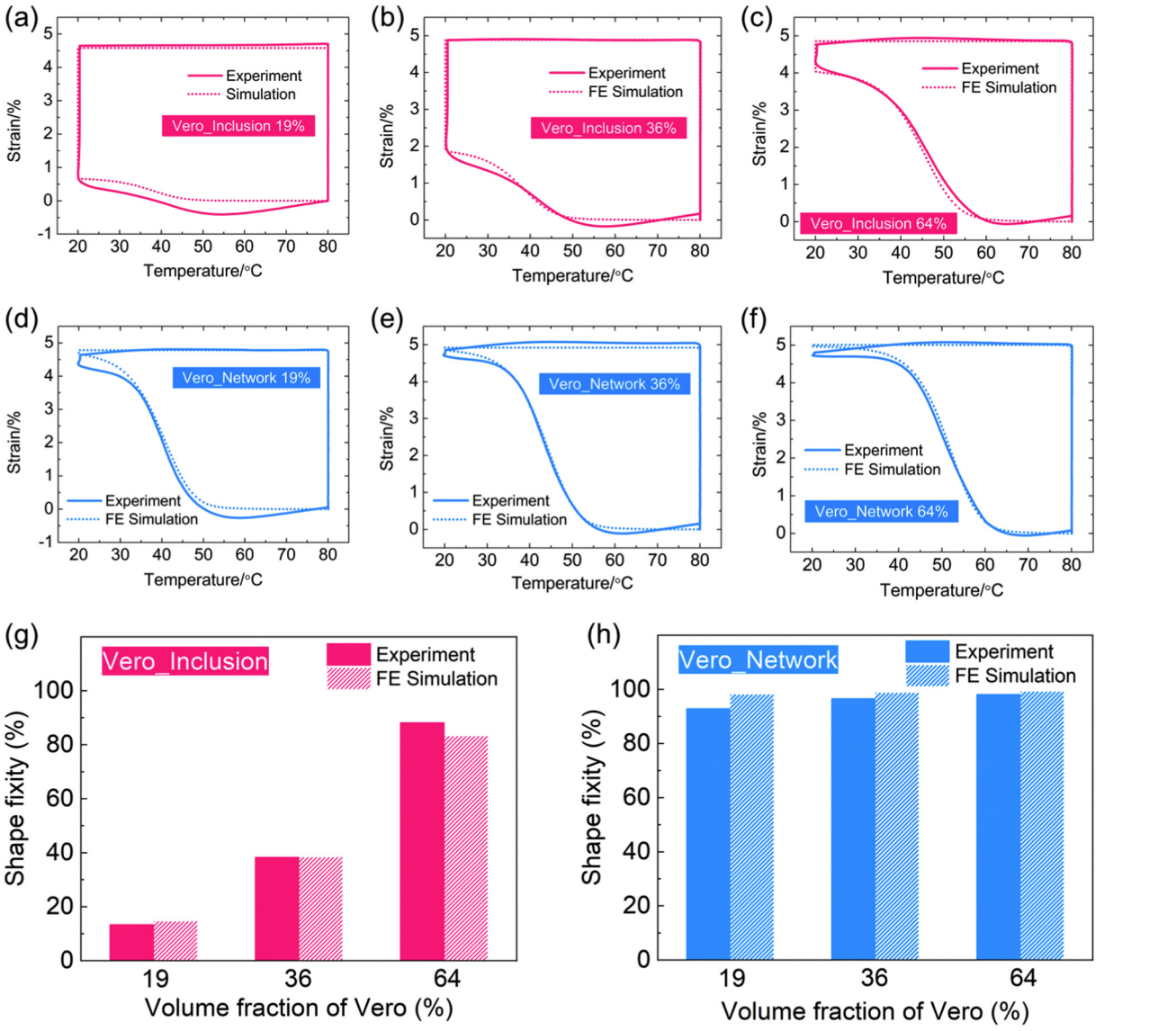


**Fig. 6.** Comparison of the shape memory property between the FE simulations and experiments. a–c) Temperature-dependent strain variation of the Vero_Inclusion samples with Vero contents of 19%, 36% and 64%. d–f) Temperature-dependent strain variation of the Vero_Network samples with Vero contents of 19%, 36% and 64%. g) Shape fixity of Vero_Inclusion samples with elevated Vero contents. g) Shape fixity of Vero_Network samples with elevated Vero contents.

Furthermore, different shape fixity variation trends with Vero content can be well predicted for two types of material layouts (Fig. 6g and h), which again validates the efficiency of the FE simulations. To provide the readers with a more intuitive expression, FE simulations of shape memory process are presented in Section S3 of the Supplementary Materials.

### 3.3. Demonstrations

So far, we have thoroughly investigated the shape memory behavior of the multi-material composites with single pattern mode of either Vero_Inclusion or Vero_Network. In the following, we investigate the shape memory performance and thermomechanical properties of the composites with multiple pattern modes. As shown in Fig. 7a and b, the Vero_Inclusion pattern and Vero_Network pattern are connected in a tandem mode with a VeroBlack volume fraction of 19%. Compared to the single pattern cases shown in Figs. 3a, 5a and b, the shape fixity and $T_g$ of the tandem sample lie between the Vero_Inclusion pattern and Vero_Network pattern. However, for the pattern in a parallel mode, the shape memory performance and thermomechanical properties shown in Fig. 7c and d are closer to the pure Vero_Network pattern where all the programmed strain is applied on the VeroBlack network along the loading direction.

In addition to being combined within the same layer, composites of different material layouts can be also stacked along the thickness direction to construct bilayer laminates capable of programmed active bending. The schematic of a bilayer laminate is shown in Fig. 8a where the Vero_Inclusion and Vero_Network layers are demonstrated with detail features. To initiate the active bending, the bilayer laminate is first stretched at high temperature $T_H$ where both layers behave in the rubbery state. Then by maintaining the programming strain $\varepsilon_0$, the laminate is cooled to $T_L$. Upon unloading, since the Vero_Inclusion layer and Vero_Network layer exhibit different shape fixity, strain mismatch is created to induce the overall bending of the bilayer laminate towards the direction of Vero_Inclusion layer. Further, if the laminate is reheated to $T_H$, the original configuration is restored due to the shape recovery of both layers.

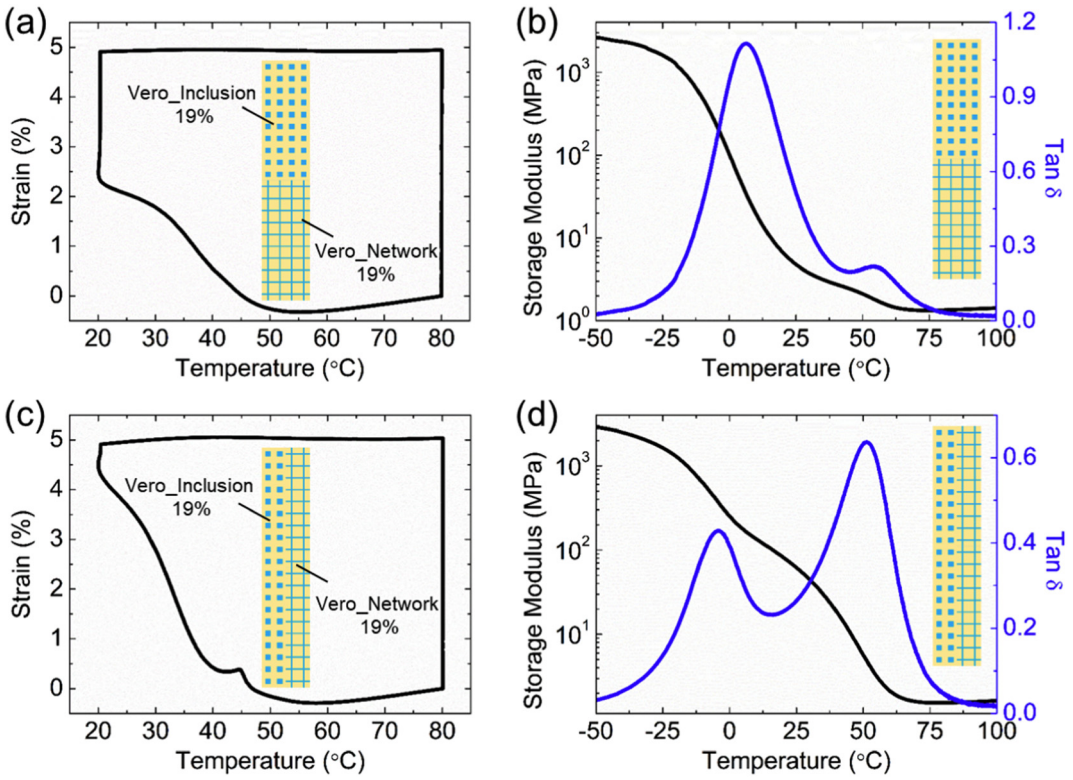


**Fig. 7.** Experimental characterizations of the shape memory performance and thermomechanical properties for the composites with multiple pattern modes. a) Shape memory performance of the composite where the Vero_Inclusion pattern and Vero_Network pattern are combined in a tandem mode. b) DMA results of the composite where the Vero_Inclusion pattern and Vero_Network pattern are combined in a tandem mode. c) Shape memory performance of the composite where the Vero_Inclusion pattern and Vero_Network pattern are combined in a parallel mode. d) DMA results of the composite where the Vero_Inclusion pattern and Vero_Network pattern are combined in a parallel mode. For all samples, the VeroBlack volume fraction is 19%.

To explore the design space of the bending angle, bilayer samples (dimension: 50 mm × 5 mm × 1 mm) with different pattern combinations were printed. Three representative VeroBlack contents (19%, 36% and 64%) were available for each layer to construct the Vero_Network or Vero_Inclusion patterns and the thickness ratio between Vero_Network layer and Vero_Inclusion layer were designed as 1/4. Following the aforementioned procedures for thermomechanical programming, bending experiments were conducted in the circulating water bath (Huber CC-118A, Peter Huber Kältemaschinenbau, Offenburg, Germany) with precise temperature control. The high temperature $T_H$, low temperature $T_L$ and programming strain $\varepsilon_0$ were respectively set as 80 °C, 20 °C and 10%. Herein, we note that for our multi-material sample, the good interfacial bonding between Vero and Tango is crucial to maintain the desired mechanical properties.

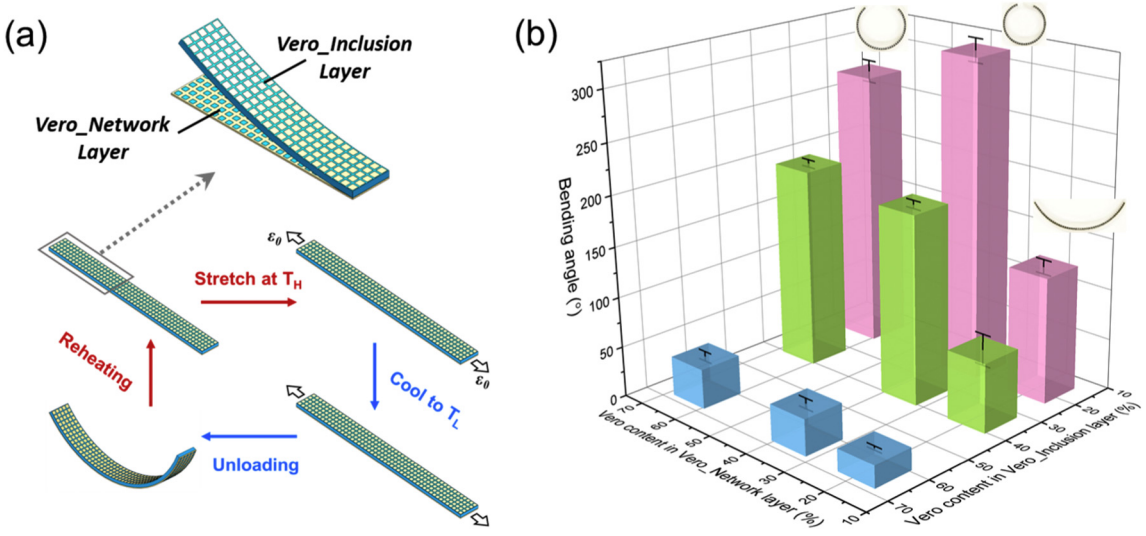


**Fig. 8.** Programmed active bending of bilayer laminate composed of Vero_Inclusion layer and Vero_Network layer. a) Schematics of the bilayer laminate and the thermomechanical programming procedures of bending actuation. b) Experimental results of the bending angle under multiple pattern combinations.

Therefore, the effect of mechanical deformation on the microstructure interface was investigated by microscopic observation. It is observed that upon applying a tensile strain, no apparent difference could be found at the interfaces, which indicates the good bonding between Vero and Tango. More details and the microscopic images are provided in Section S4 of the Supplementary Materials.

Experimental results of the bending angle under different pattern combinations are shown in Fig. 8b. When the VeroBlack content is fixed in the Vero_Network layer, bending angle of the bilayer laminate is monotonically decreased by raising the VeroBlack content in the Vero_Inclusion layer. This trend can be easily understood by considering the positive correlation between the VeroBlack content and the shape fixity of the Vero_Inclusion pattern, as demonstrated in Fig. 3. Upon increasing the VeroBlack content, the shape fixity of the Vero_Inclusion layer is gradually enhanced to diminish the strain mismatch relative to the Vero_Network layer, which accordingly yields a reduced bending angle.

On the other hand, when the VeroBlack content is fixed in the Vero_Inclusion layer, there is an optimal VeroBlack content in the Vero_Network layer to realize the maximum bending angle. This is a combined effect induced by the shape fixity gap and the stiffness compatibility between the two layers. For a Vero_Network layer with low VeroBlack content (for instance, 19%), finite strain recovery exists upon unloading, which accordingly reduces the strain mismatch relative to the Vero_Inclusion layer. However, if the VeroBlack content is too high (for instance, 64%), the Vero_Network layer may become too stiff to be pulled by the Vero_Inclusion layer with a shrinkage tendency. Therefore, a maximum bending angle is provided by using a medium VeroBlack content in the Vero_Network layer.

## 4. Discussion

With the experimental results presented above, some potential applications are readily proposed for the multi-material composites of different patterns according to their respective thermomechanical characteristics.

As shown in Figs. 3 and 5, with the increase of VeroBlack content, the shape fixity of the Vero_Network pattern maintains at a high level (over 90%) whereas the elastic modulus monotonically increases. Therefore, the Vero_Network pattern provides a convenient strategy of creating shape memory materials with tunable elastic modulus.

For Vero_Inclusion pattern, since the $T_g$ of the composite gradually increases with the VeroBlack content (Fig. 5), a series of materials with elevated $T_g$ are available, which can be implemented into a single structure to realize sequential shape recovery [39].

Although only two representative patterns are focused in this work, we have successfully demonstrated that with two base materials, we are capable of customizing a number of shape memory properties with rational pattern design. Also, in addition to the Polyjet 3D printing technology used in this work, our pattern design idea is applicable to other multimaterial 3D printing technology including DLP [19,20] 3D printing and direct ink write (DIW) 3D printing [40]. In spite of this, many design possibilities still exist to achieve multi-purpose material customizations, such as giving consideration to both the shape memory performance and fracture toughness. Therefore, more combinations of base materials and pattern modes are required to be explored in the future study.

## 5. Conclusion

In this paper, a pattern design based strategy is proposed to regulate the shape memory performance of multi-material composites. Two representative patterns including Vero_Network mode and Vero_Inclusion mode are respectively demonstrated to investigate the effect of VeroBlack volume fraction on the shape fixity of the composite. For the Vero_Network pattern, the shape fixity maintains at a high level (over 90%) regardless of the VeroBlack volume fraction. In contrast, the shape fixity of the Vero_Inclusion pattern shows a positive correlation with the VeroBlack volume fraction. In addition, composites with multiple pattern modes are investigated by combing the Vero_Network and Vero_Inclusion patterns in series or in parallel. Compared to the single pattern case with identical VeroBlack content, the tandem sample possesses properties in between whereas the parallel mode is closer to the Vero_Network pattern. At last, a 4D printing demonstration is presented by stacking Vero_Inclusion pattern and Vero_Network pattern into a bilayer laminate to realize programmed active bending. By varying the VeroBlack content in the Vero_Inclusion or Vero_Network layer, a broad range of bending curvature is available.

Supplementary data to this article can be found online at https://doi.org/10.1016/j.matdes.2020.108785.

## CRediT authorship contribution statement

**Chao Yuan:** Conceptualization, Methodology, Investigation, Writing - original draft. **Fangfang Wang:** Methodology, Investigation, Visualization. **Biyun Qi:** Investigation. **Zhen Ding:** Methodology, Investigation. **David W. Rosen:** Supervision, Writing - review & editing, Funding acquisition. **Qi Ge:** Supervision, Writing - review & editing.

## Declaration of competing interest

The authors declare that they have no known competing financial interests or personal relationships that could have appeared to influence the work reported in this paper.

## Acknowledgements

We gratefully acknowledge the grants (RGDM1710205, RGDM1830501 and RGDM1830206) from SUTD Digital Manufacturing and Design Centre (DManD) funded by the Singapore National Research Foundation. F.W. acknowledges the support by the NSFC (No. 11802233). Z.D. acknowledges supports by the NSFC (No. 11872369) and the Key Field R & D Program of Guangdong Province (2019B010941001). Q.G. acknowledges the research startup grant (Y01336121) by Shenzhen Municipal Government and the research startup grant (Y01336221) support by Southern University of Science and Technology.

## Data availability

The raw and processed data required to reproduce these findings cannot be shared at this time as the data also forms part of an ongoing study.

## References

[1] Q. Zhao, H.J. Qi, T. Xie, Recent progress in shape memory polymer: new behavior, enabling materials, and mechanistic understanding, Prog. Polym. Sci. 49–50 (2015) 79–120.

[2] M. Lei, Z. Chen, H. Lu, K. Yu, Recent progress in shape memory polymer composites: methods, properties, applications and prospects, Nanotechnol. Rev. 8 (1) (2019) 327–351.

[3] A. Lendlein, O.E.C. Gould, Reprogrammable recovery and actuation behaviour of shape-memory polymers, Nat Rev Mater 4 (2) (2019) 116–133.

[4] C. Yuan, Z. Ding, T.J. Wang, M.L. Dunn, H.J. Qi, Shape forming by thermal expansion mismatch and shape memory locking in polymer/elastomer laminates, Smart Mater. Struct. 26 (10) (2017), 105027. .

[5] M. Zarek, M. Layani, I. Cooperstein, E. Sachyani, D. Cohn, S. Magdassi, 3D printing of shape memory polymers for flexible electronic devices, Adv. Mater. 28 (22) (2016) 4449–4454.

[6] X.J. Wang, X.G. Guo, J.L. Ye, N. Zheng, P. Kohli, D.W. Cho, Y. Zhang, Z.Q. Xie, Q.H. Zhang, H.W. Luan, K.W. Nan, B.H. Kim, Y.M. Xu, X.W. Shan, W.B. Bai, R.J. Sun, Z.Z. Wang, H.Y. Jang, F. Zhang, Y.J. Ma, Z. Xu, X. Feng, T. Xie, Y.G. Huang, Y.H. Zhang, J.A. Rogers, Freestanding 3D mesostructures, functional devices, and shape-

programmable systems based on mechanically induced assembly with shape memory polymers, Adv. Mater. 31 (2) (2019) 1805615.
[7] Y.F. Zhang, N.B. Zhang, H. Hingorani, N.Y. Ding, D. Wang, C. Yuan, B. Zhang, G.Y. Gu, Q. Ge, Fast-response, stiffness-tunable soft actuator by hybrid multimaterial 3D printing, Adv. Funct. Mater. 29 (15) (2019), 1806698. .
[8] Q.J. Ze, X. Kuang, S. Wu, J. Wong, S.M. Montgomery, R.D. Zhang, J.M. Kovitz, F.Y. Yang, H.J. Qi, R.K. Zhao, Magnetic shape memory polymers with integrated multifunctional shape manipulation, Adv. Mater. 32 (4) (2020) 1906657.
[9] B.J. Jin, H.J. Song, R.Q. Jiang, J.Z. Song, Q. Zhao, T. Xie, Programming a crystalline shape memory polymer network with thermo- and photo-reversible bonds toward a single-component soft robot, Sci. Adv. 4 (1) (2018) eaao3865.
[10] C. Lin, J.X. Lv, Y.S. Li, F.H. Zhang, J.R. Li, Y.J. Liu, L.W. Liu, J.S. Leng, 4D-printed biodegradable and remotely controllable shape memory occlusion devices, Adv. Funct. Mater. 29 (51) (2019) 1906569.
[11] A. Lendlein, R. Langer, Biodegradable, elastic shape-memory polymers for potential biomedical applications, Science 296 (5573) (2002) 1673–1676.
[12] C.M. Yakacki, R. Shandas, D. Safranski, A.M. Ortega, K. Sassaman, K. Gall, Strong, tailored, biocompatible shape-memory polymer networks, Adv. Funct. Mater. 18 (16) (2008) 2428–2435.
[13] D.L. Safranski, K. Gall, Effect of chemical structure and crosslinking density on the thermo-mechanical properties and toughness of (meth)acrylate shape memory polymer networks, Polymer 49 (20) (2008) 4446–4455.
[14] T. Xie, I.A. Rousseau, Facile tailoring of thermal transition temperatures of epoxy shape memory polymers, Polymer 50 (8) (2009) 1852–1856.
[15] Y.Y.C. Choong, S. Maleksaeedi, H. Eng, J. Wei, P.C. Su, 4D printing of high performance shape memory polymer using stereolithography, Mater. Design. 126 (2017) 219–225.
[16] H.Z. Wu, P. Chen, C.Z. Yan, C. Cai, Y.S. Shi, Four-dimensional printing of a novel acrylate-based shape memory polymer using digital light processing, Mater. Design. 171 (2019) 107704.
[17] X. Li, Y. Yang, Y. Zhang, T. Wang, Z. Yang, Q. Wang, X. Zhang, Dual-method molding of 4D shape memory polyimide ink, Mater. Design. 191 (2020) 108606.
[18] S.Y. Chen, Q.L. Zhang, J.C. Feng, 3D printing of tunable shape memory polymer blends, J. Mater. Chem. C 5 (33) (2017) 8361–8365.
[19] Q. Ge, A.H. Sakhaei, H. Lee, C.K. Dunn, N.X. Fang, M.L. Dunn, Multimaterial 4D printing with tailorable shape memory polymers, Sci. Rep. 6 (2016), 31110. .
[20] K. Kowsari, S. Akbari, D. Wang, N.X. Fang, Q. Ge, High-efficiency high-resolution multimaterial fabrication for digital light processing-based three-dimensional printing, 3D Print Addit. Manuf. 5 (3) (2018) 185–193.
[21] D. Kokkinis, F. Bouville, A.R. Studart, 3D printing of materials with tunable failure via bioinspired mechanical gradients, Adv. Mater. 30 (19) (2018), 1705808. .
[22] L.Q. Ren, Z.Y. Song, H.L. Liu, Q.H. Han, C. Zhao, B. Derby, Q.P. Liu, L. Ren, 3D printing of materials with spatially non-linearly varying properties, Mater. Design. 156 (2018) 470–479.
[23] X. Kuang, J.T. Wu, K.J. Chen, Z. Zhao, Z. Ding, F.J.Y. Hu, D.N. Fang, H.J. Qi, Grayscale digital light processing 3D printing for highly functionally graded materials, Sci. Adv. 5 (5) (2019) eaav5790.
[24] Y. Zhang, L.M. Huang, H.J. Song, C.J. Ni, J.J. Wu, Q. Zhao, T. Xie, 4D printing of a digital shape memory polymer with tunable high performance, ACS. Appl. Mater. Inter. 11 (35) (2019) 32408–32413.
[25] G. Sossou, F. Demoly, H. Belkebir, H.J. Qi, S. Gomes, G. Montavon, Design for 4D printing: modeling and computation of smart materials distributions, Mater. Design. 181 (2019) 108074.
[26] G. Sossou, F. Demoly, H. Belkebir, H. Qi, S. Gomes, G. Montavon, Design for 4D printing: a voxel-based modeling and simulation of smart materials, Mater. Design. 175 (2019) 107798.
[27] C. Yuan, T.J. Wang, M.L. Dunn, H.J. Qi, 3D printed active origami with complicated folding patterns, Int. J. Pr. Eng. Man.-GT 4 (3) (2017) 281–289.
[28] Z. Ding, C. Yuan, X.R. Peng, T.J. Wang, H.J. Qi, M.L. Dunn, Direct 4D printing via active composite materials, Sci. Adv. 3 (4) (2017), e1602890. .
[29] Q. Ge, C.K. Dunn, H.J. Qi, M.L. Dunn, Active origami by 4D printing, Smart Mater. Struct. 23 (9) (2014), 094007. .
[30] F. Momeni, N.S.M.M. Hassani, X. Liu, J. Ni, A review of 4D printing, Mater. Design. 122 (2017) 42–79.
[31] M. Bodaghi, A.R. Damanpack, W.H. Liao, Self-expanding/shrinking structures by 4D printing, Smart Mater. Struct. 25 (10) (2016), 105034. .
[32] M. Bodaghi, A.R. Damanpack, W.H. Liao, Triple shape memory polymers by 4D printing, Smart Mater. Struct. 27 (6) (2018), 065010. .
[33] F. Wang, C. Yuan, D. Wang, D.W. Rosen, Q. Ge, A phase evolution based constitutive model for shape memory polymer and its application in 4D printing, Smart Mater. Struct. 29 (5) (2020), 055016. .
[34] C. Yuan, X.M. Mu, C.K. Dunn, J. Haidar, T.J. Wang, H.J. Qi, Thermomechanically triggered two-stage pattern switching of 2D lattices for adaptive structures, Adv. Funct. Mater. 28 (18) (2018), 1705727. .
[35] M. Bodaghi, A.R. Damanpack, W.H. Liao, Adaptive metamaterials by functionally graded 4D printing, Mater. Design. 135 (2017) 26–36.
[36] P. Zhang, M.A. Heyne, A.C. To, Biomimetic staggered composites with highly enhanced energy dissipation: modeling, 3D printing, and testing, J. Mech. Phys. Solids. 83 (2015) 285–300.
[37] V. Slesarenko, N. Kazarinov, S. Rudykh, Distinct failure modes in bio-inspired 3D-printed staggered composites under non-aligned loadings, Smart Mater. Struct. 26 (3) (2017), 035053. .
[38] K.K. Westbrook, P.H. Kao, F. Castro, Y.F. Ding, H.J. Qi, A 3D finite deformation constitutive model for amorphous shape memory polymers: a multi-branch modeling approach for nonequilibrium relaxation processes, Mech. Mater. 43 (12) (2011) 853–869.
[39] Y.Q. Mao, K. Yu, M.S. Isakov, J.T. Wu, M.L. Dunn, H.J. Qi, Sequential self-folding structures by 3D printed digital shape memory polymers, Sci. Rep. 5 (2015) 13616.
[40] M.A. Skylar-Scott, J. Mueller, C.W. Visser, J.A. Lewis, Voxelated soft matter via multimaterial multinozzle 3D printing, Nature 575 (7782) (2019) 330–335.